EVALUATION OF SINTERED PROPERTIES OF PM STEELS BASED ON Cr AND Cr-Mn PREALLOYED STEEL POWDERS

O. Bergman, L. Nyborg

Abstract

Increased use of the effective and low cost alloying elements Cr and Mn in PM steel requires enhanced knowledge regarding sintering of such alloys. In this study, sintered properties of PM steels based on 1.8% Cr and 0.8% Cr-0.4% Mn prealloyed steel powders are evaluated. Both materials obtain, with 0.7% C, fine pearlitic microstructures after sintering at 1120-1250°C in N2/H2 (90/10) followed by normal cooling (0.5-1°C/s). These structures provide attractive combinations of strength and ductility. The materials gain considerably in mechanical performance with higher sintering temperature mainly due to increased sinter neck contact area and pore rounding effects. Mechanical properties of the materials are also significantly improved with increasing specimen density throughout the density range 7.0-7.6 g/cm^3. Submicron residual oxides of Cr-Mn rich spinel type are found in the materials after sintering at 1120°C. Application of higher sintering temperatures (1200/1250°C) leads to reduction of such oxides through more active carbothermal reduction mechanisms locally in the materials. However, high density (7.5-7.6 g/cm^3) specimens contain small residual oxide particles also after high temperature sintering due to pore closure during sintering. The residual oxides have no obvious detrimental effect on mechanical properties of the PM steels.

Keywords: PM steel, chromium, manganese, prealloyed powder, sintering, sintering temperature, specimen density, mechanical properties, oxide reduction, spinel oxide

INTRODUCTION

The powder metallurgy (PM) industry has experienced very strong growth in the past few decades. This growth is mainly attributed to the cost efficiency of the PM process compared to conventional technologies (casting and forging) in production of structural steel components. However, high and volatile prices of the most commonly used alloying elements (Ni, Mo, Cu) in PM steel are today threatening to hinder continued growth of the PM industry. Therefore, increased use of low cost and effective alloying elements, such as Cr and Mn, is crucial for maintaining the cost advantage of PM components over conventional steel components. The oxidation sensitivity of Cr and Mn has historically been a limiting factor for using these elements in PM applications, but improvements in production processes for powders and PM components have changed the situation. Water-atomized steel powder grades prealloyed with Cr (1.5-3%) and low amounts of Mo (0.2-0.5%) have now been available on the market for some years, and these materials can be

Ola Bergman Global Development, Höganäs AB, Höganäs, Sweden
Lars Nyborg Department of Materials and Manufacturing Technology, Chalmers University of Technology, Gothenburg, Sweden

applied in a conventional press-sinter process route to reach the mechanical properties needed for high performance applications [1-4]. The key for successful processing of these types of powder alloys is a well-controlled sintering process. Sintering atmosphere with low oxygen content, preferably a high purity N_2/H_2 mix, must be used in order to have reducing conditions. Furthermore, an appropriate temperature cycle should be applied to ensure that sufficient reduction of oxides on the powder surfaces takes place in the process.

Two kinds of newly developed water-atomized steel powder, one prealloyed with 1.8% Cr and the other with 0.8% Cr and 0.4% Mn, have been shown to offer good combinations of strength and ductility in PM steel [5]. These powder grades are studied further in this investigation. Mechanical properties are evaluated after compaction of powder mixes (containing 0.8% graphite) into test bars with different densities (7.0-7.5 g/cm^3) followed by sintering at temperatures of between 1120°C and 1250°C in N_2/H_2 atmosphere. Oxide reduction during sintering is considered, with emphasis on influence of specimen porosity and sintering temperature, given the high thermodynamic stability of oxides in alloys containing Cr and Mn. Furthermore, residual oxides in the sintered specimens are examined and their effect on the mechanical performance of the materials is discussed. The reference material included in the investigation is a water-atomized steel powder grade prealloyed with 1.5% Mo, i.e. a material without oxidation sensitive alloying elements.

OXIDE REDUCTION DURING SINTERING

Water-atomized and subsequently annealed steel powder is to the largest extent covered by a thin surface oxide layer, but there are also particulate oxide features present to a minor part. The composition, morphology and thickness of the surface oxides are decided by the alloy composition of the powder and the process parameters in the production process. Steel powder prealloyed with 1.5-3% Cr and 0.2-0.5% Mo have surface oxide particles (up to about 0.2 μm in size) that are rich in Cr and other strong oxide formers (Mn, Si) evenly distributed on the surfaces, and these particles are surrounded by a continuous Fe oxide layer with a thickness of 6-7 nm [6-7]. Similar surface oxides have been shown to exist on steel powder prealloyed with 0.3-1.8% Mn and up to 0.3% Cr, although the oxide particles are richer in Mn and contain less Cr on these powders than on the Cr-Mo prealloyed powders [8]. Consequently, water-atomized steel powders that are prealloyed with Cr and/or Mn display some enrichment of these elements and other oxidation sensitive impurity elements (e.g. Si) at the powder surfaces, where they form small (submicron) oxide particulate features. In this context, it should be emphasized that also gas-atomized powder show similar characteristics [9-10].

Bonding between the steel powder particles in pressed PM compacts during sintering occurs through diffusion processes. Hence, surface oxide layers on the powder particles have to be reduced at least partially in order to ensure the necessary metal-to-metal contact between particles for efficient sinter neck formation. The possibility to reduce the surface oxides is determined by the thermodynamic stability of the different oxide phases present and by the applied temperature cycle and atmosphere composition in the sintering process. Moreover, the porosity level of the PM compacts and component size are factors that might affect the oxide reduction due to their influence on the gas transport processes inside the compacts.

Accurate predictions of oxide stabilities in alloy steel require reliable thermodynamic data for the material system in question. A thermodynamic description of the Fe-C-Cr-Mn-Ni-O system has been developed recently, with new and improved data for mixed Fe-Cr-Mn oxides [11]. This description is incorporated in the thermodynamic steel

database TCFE6.2, which has been used here together with the software Thermo-Calc to perform calculations for the two alloys that are studied in the investigation. Calculation results for the typical sintering temperature 1120°C show that spinel (M_3O_4, where M is one or more of Fe, Cr, Mn) is the most stable oxide phase for both alloy compositions (see Fig.1). Hence, stable oxide particulate features on the powder surfaces of these alloys are likely to be of spinel type. The equilibrium composition of the spinel oxide changes with the oxygen partial pressure at fixed temperature, going from $MnCr_2O_4$ at the lowest p_{O2} to mixed $(Fe,Cr,Mn)_3O_4$ type at higher oxygen pressures. The spinel changes relatively fast to Cr-Fe rich with higher p_{O2} for the Fe-1.8% Cr-0.1% Mn alloy, while the spinel is Cr-Mn rich almost throughout the entire p_{O2} stability range for the Fe-0.8% Cr-0.4% Mn alloy. The halite phase that appears at $p_{O2} > 10^{-13}$ atm is basically FeO, but it also contains small amounts of Cr and Mn. The results in Fig.1 also demonstrate that pO2 in the sintering atmosphere should be below $3 \cdot 10^{-18}$ atm at 1120°C in order to have reducing conditions for the spinel oxide in both materials. Similar critical oxygen pressure for oxide reduction has been reported for sintering of steel powder prealloyed with 3% Cr [12]. Conditions are reducing at higher p_{O2} values in the atmosphere during high temperature sintering, which is typically done at temperatures above 1200°C, since the oxide stability decreases with increasing temperature.

Besides favourable thermodynamic conditions, reduction media have to be available for removal of the oxides. In the sintering process, metal oxide (M_xO_y) reduction occurs either through interaction with H_2 in the atmosphere according to reaction (1), or via carbothermal reduction through interaction with C in the material according to reactions (2) and (3).

$$M_xO_y(s) + yH_2(g) \rightarrow xM(s) + yH_2O(g) \quad (1)$$
$$M_xO_y(s) + yC(s) \rightarrow xM(s) + yCO(g) \quad (2)$$
$$M_xO_y(s) + yCO(g) \rightarrow xM(s) + yCO_2(g) \quad (3)$$

The carbothermal reduction starts in accordance with reaction (2) when the temperature is high enough to activate the carbon in the powder compact. However, as soon as CO becomes available reaction (3) will be the dominating reduction mechanism, and regeneration of CO is ensured at high temperatures by the Boudouard reaction [13-15]:

$$C(s) + CO_2(g) \rightarrow 2CO(g) \quad (4)$$

Oxide reduction mechanisms during sintering of PM compacts based on powder prealloyed with 3% Cr and 0.5% Mo have been studied in several investigations [16-19]. These studies show that H_2 reduction of iron oxides on the powder surfaces occurs in the temperature range of 300-600°C during heating in N_2/H_2 atmosphere. Carbothermal reduction is initiated at around 700°C, which is attributed to further iron surface oxide reduction. More intense carbothermal reduction takes place above ~900°C when stable Cr-containing oxides on the powder surfaces are reduced. Reduction maxima for these oxides are obtained at 1000-1050°C and 1200-1250°C. Similar oxide reduction sequence has been reported from sintering trials of PM compacts based on powder prealloyed with 0.3-1.2% Cr and 0.8-1.2% Mn [20]. In this case, large carbothermal reduction peaks with maxima at 1200-1250°C are obtained due to removal of stable Cr-Mn oxides.

All of the mentioned studies of oxide reduction during sintering were performed on test specimens with density around 7.0 g/cm^3, which means that there is open and interconnected porosity in the PM compacts that allows transport of the gas species that

take part in the reduction reactions (1)-(3). In another investigation, oxide reduction during sintering of high density (7.5-7.6 g/cm^3) PM compacts based on powder prealloyed with 1.5% Cr and 0.2% Mo was studied [21]. The oxide reduction in these specimens is virtually stopped at temperatures above 1150°C due to closing of the pore channels, and thereby stable Cr oxides remain in the material even after heating to 1300°C. The compact density above which there is no open porosity after sintering at 1120-1250°C is around 7.45-7.5 g/cm^3 for a Cr-Mo powder alloy according to a recent study [22].

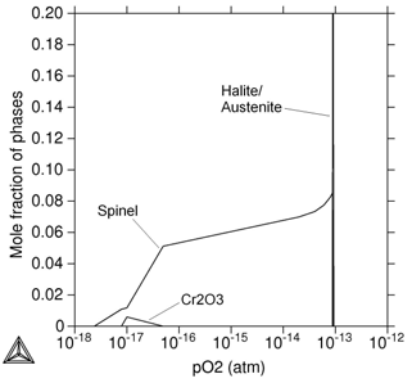

a) Mole fraction of phases vs. p_{O2} for Fe-1.8% Cr-0.1%Mn at 1120°C.

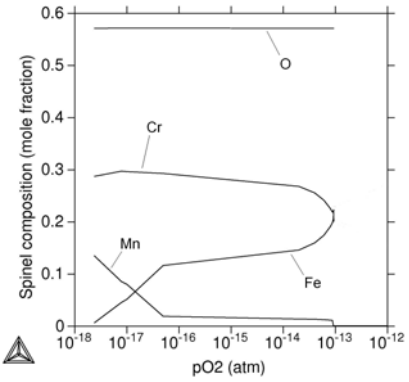

b) Composition of spinel phase vs. p_{O2} for Fe-1.8% Cr-0.1% Mn at 1120°C.

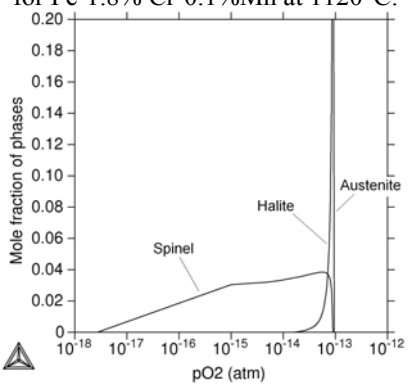

c) Mole fraction of phases vs. p_{O2} for Fe-0.8% Cr-0.4% Mn at 1120°C.

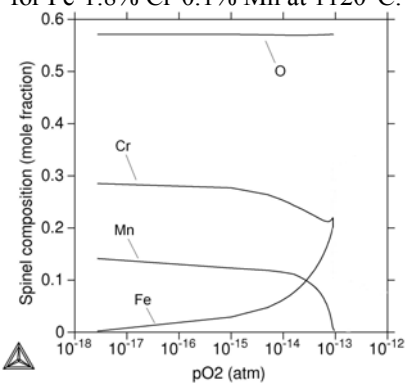

d) Composition of spinel phase vs. p_{O2} for Fe-0.8% Cr-0.4% Mn at 1120°C.

Fig.1. Results from calculations with Thermo-Calc software and TCFE6.2 database.

EXPERIMENTAL PROCEDURE

Two kinds of water-atomized steel powder, one prealloyed with 1.8% Cr (Powder A) and the other prealloyed with 0.8% Cr and 0.4% Mn (Powder B), were used as test materials. The water-atomized steel powder grade Astaloy Mo (Powder C), which is prealloyed with 1.5% Mo, was included in the study as reference material. The chemical compositions of the investigated powders are given in Table 1.

Each powder was mixed with 0.8% graphite (Kropfmühl UF4) and lubricant (0.6% Kenolube or 0.5% Lube E) in a laboratory batch mixer. Two premixes (one for each lubricant) were made for all three kinds of powder. Standard tensile test specimens (ISO

2740-1986) and un-notched impact test specimens (ISO 5754) with three different density levels were produced by cold compaction with 600 MPa compaction pressure, compaction at 800 MPa with heated (80°C) tool, and double pressing with compaction pressures 700/900 MPa, respectively. The specimens were pre-sintered at 750°C for 30 minutes in $75H_2/25N_2$ between the two compaction steps in the double pressing operation. Chemical analyses showed that there was no oxidation of the specimens during pre-sintering. The mixes containing Lube E were used for compaction with heated tool, while the mixes containing Kenolube were used for the other pressing operations. Specimen green densities obtained for the different materials are presented in Table 2.

Tab.1. Chemistry of investigated prealloyed powder grades.

Powder	Fe [%]	Cr [%]	Mn [%]	Mo [%]	O [%]	C [%]
A	Base	1.80	0.10	0.02	0.14	<0.01
B	Base	0.82	0.39	0.03	0.13	<0.01
C	Base	0.03	0.13	1.53	0.09	<0.01

Tab.2. Green densities of tensile test specimens after different pressing operations. (CC = cold compaction, HTC = heated tool compaction, DP = double pressing)

Material	Powder	C-UF4 [%]	Green density [g/cm^3]		
			CC – 600 MPa	HTC – 800 MPa	DP - 700/900 MPa
A-08C	A	0.8	6.99	7.23	7.54
B-08C	B	0.8	7.05	7.28	7.54
C-08C	C	0.8	7.06	7.31	7.54

Test specimens of all material types and density levels were sintered for 30 minutes at three different temperatures (1120/1200/1250°C). The sintering at 1120°C was done in a laboratory mesh belt furnace, while the sintering at 1200°C and 1250°C were done in a laboratory batch furnace. All specimens from the high temperature sintering were re-sintered in the mesh belt furnace (1120°C for 30 min) in order to ensure that the same cooling rate after sintering was applied for all materials. This cooling rate was between 0.5°C/s and 1°C/s in the temperature range 300-800°C. High purity $90N_2/10H_2$ gas mixture (dew point < -40°C) was used as protective atmosphere in all sintering processes. The dew point corresponds to a partial pressure of oxygen of $< 3 \cdot 10^{-19}$ atm at 1120°C. This atmosphere is reducing for the investigated alloys at all three sintering temperatures (c.f. Fig.1).

Tensile testing of the sintered specimens was performed in a Zwick Z100 machine and Charpy impact tests were done in accordance with standard EN 10045-1. Hardness was measured on specimen surfaces through the Vickers method. Microstructures were examined by light optical microscopy (LOM) and fracture surfaces of tensile specimens were studied by high resolution scanning electron microscopy (HR-SEM) in a LEO Gemini 1550 instrument. Particulate features in the fracture surfaces were analyzed by energy dispersive X-ray spectroscopy (EDX) through an INCA system in combination with the SEM instrument. Bulk oxygen and carbon concentrations of the sintered specimens were measured through infrared (IR) technique in LECO instruments. Dimensional change during sintering was determined from die to sintered size on tensile specimens. Sintered density was measured on tensile specimens by using hydrostatic weighing in accordance with standard ISO 2738:2000.

RESULTS

Dimensional change (DC) and density data for the sintered materials are presented in Table 3. It should be noted that DC is measured from die to as-sintered, which means that spring back after pressing of up to ~0.3% is included in the values. Therefore, most specimens have experienced shrinkage during sintering, although the DC values are positive. Material A-08C displays most shrinkage and material C-08C least shrinkage during sintering. Sintered densities are 7.0-7.1 g/cm^3 for the cold compacted materials, around 7.3 g/cm^3 for the materials compacted with heated tool, and 7.5-7.6 g/cm^3 for the double pressed materials. Gain in density with higher sintering temperature is 0.02-0.06 g/cm^3 (1200°C) and 0.03-0.08 g/cm^3 (1250°C) compared to 1120°C, except for the double pressed materials where the density gain generally is lower.

Tab.3. Dimensional changes (DC – measured from die) and sintered density (SD) after sintering for 30 min at T in $90N_2/10H_2$ atmosphere.

Material	Pressing	T = 1120°C		T = 1200°C		T = 1250°C	
		DC [%]	SD [g/cm^3]	DC [%]	SD [g/cm^3]	DC [%]	SD [g/cm^3]
A-08C	CC	0.076	7.00	-0.248	7.06	-0.472	7.08
	HTC	0.142	7.23	-0.110	7.28	-0.288	7.30
	DP	0.443	7.52	0.318	7.56	0.214	7.56
B-08C	CC	0.137	7.07	-0.030	7.09	-0.215	7.12
	HTC	0.180	7.28	0.030	7.31	-0.113	7.34
	DP	0.436	7.52	0.371	7.53	0.301	7.53
C-08C	CC	0.252	7.08	0.062	7.10	-0.106	7.12
	HTC	0.298	7.31	0.114	7.33	0.003	7.34
	DP	0.507	7.50	0.379	7.49	0.312	7.49

Materials A-08C and B-08C have similar bulk oxygen contents after sintering, as illustrated by the graphs in Fig.2. The specimen density level has no significant influence on the oxygen content in the range 7.0-7.3 g/cm^3. These specimens contain 0.04-0.05% O after 1120°C sintering, about 0.02% O after 1200°C sintering, and below 0.01% O after 1250°C sintering. The high density (7.5-7.6 g/cm^3) specimens have higher oxygen contents than the specimens with lower densities after each sintering process. They contain 0.08-0.09% O after 1120°C sintering and, in the case of material A-08C, only slightly less (0.07-0.08% O) after sintering at the higher temperatures. The high density specimens of material B-08C contain 0.05-0.06% O after the 1200°C and 1250°C sintering. The specimens of material C-08C contain ≤0.01% O at all density levels after all three sintering processes.

The carbon concentrations of the test specimens after sintering at 1120°C are 0.70-0.73% C for material A-08C and 0.68-0.71% C for material B-08C, with no significant variation between specimens of different densities. After the sintering at 1200°C and 1250°C, materials A-08C and B-08C have comparable carbon concentrations of 0.64-0.68% C for specimen densities ≤7.3g/cm^3 and 0.68-0.71% C for specimen densities ≥7.5g/cm^3. The C-08C specimens have roughly the same carbon content in the range 0.69-0.72% C after all three sintering processes and for all specimen densities.

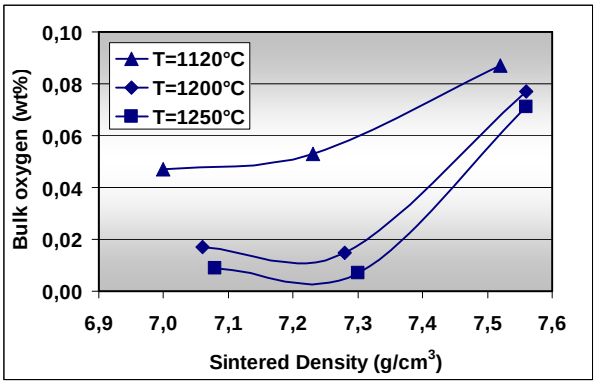

a) material A-08C

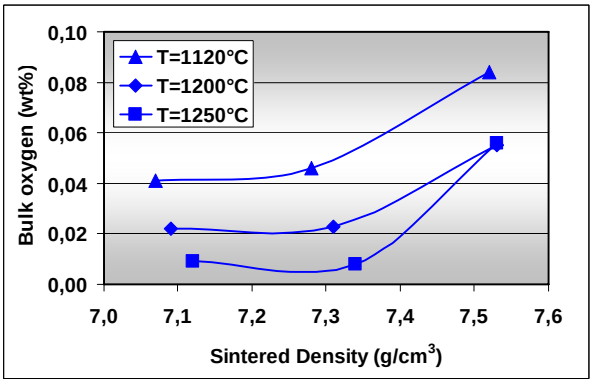

b) material B-08C

Fig.2. Bulk oxygen content in test specimens after sintering for 30 min at T in $90N_2/10H_2$ atmosphere

Mechanical properties

Specimen hardness values obtained after sintering at 1120°C are presented in Fig.3. Material A-08C has the highest hardness of the three materials, with values between 184 HV10 at density 7.0 g/cm^3 and 263 HV10 at density 7.5 g/cm^3. Corresponding hardness ranges for the other materials are 167-220 HV10 (B-08C) and 176-216 HV10 (C-08C) in the density interval 7.1-7.5 g/cm^3. Compared to the 1120°C sintering, the hardness is 3-7% higher for the A-08C specimens, 5-13% higher for the B-08C specimens and 2-10% higher for the C-08C specimens after the sintering at 1200°C and 1250°C. There is no significant difference in material hardness values between the two high temperature sintering.

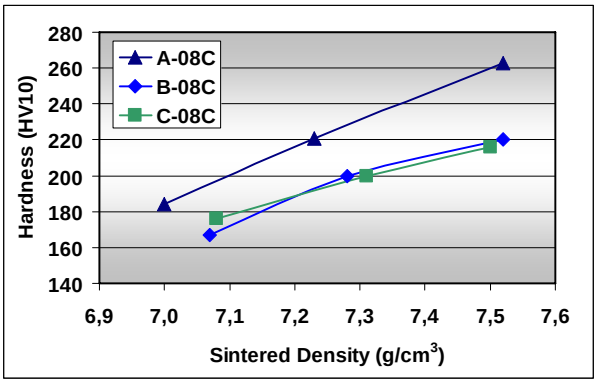

Fig.3. Specimen hardness values obtained after sintering for 30 min at 1120°C in $90N_2/10H_2$ atmosphere.

The influence of specimen density and sintering temperature on ultimate tensile strength (UTS) and yield strength (YS) of the sintered materials is given by graphs a-c in Fig.4. For material A-08C, the UTS increases from 650 MPa at density 7.0 g/cm^3 to 960 MPa at density 7.5 g/cm^3 after sintering at 1120°C. The UTS values of A-08C are 5-10% higher at each density level when the sintering temperature is raised from 1120°C to 1200°C. The same gain in UTS is achieved when the sintering temperature is raised from 1200°C to 1250°C, except at the highest density level where UTS is just above 1000 MPa in both cases. The YS of material A-08C is about 490 MPa at the lowest density level (7.0-7.1 g/cm^3) for all three sintering temperatures. At the next density level (7.2-7.3 g/cm^3), the YS is 535-540 MPa after sintering at 1120/1200°C and 580 MPa after sintering at 1250°C. For the highest specimen densities (7.5-7.6 g/cm^3), the YS of A-08C is 615 MPa after sintering at 1120°C and in the range 660-680 MPa after sintering at 1200/1250°C.

The UTS of material B-08C increases from 595 MPa at density 7.1 g/cm^3 to 830 MPa at density 7.5 g/cm^3 after sintering at 1120°C. The gain in UTS at each density level is 5-10% when the sintering temperature is raised from 1120°C to 1200°C. Corresponding gain in UTS is smaller (1-5%) when the sintering temperature is raised from 1200°C to 1250°C. The YS of material B-08C is 420-440 MPa at density 7.1 g/cm^3, 480-500 MPa at density 7.3 g/cm^3, and 505-540 MPa at density 7.5 g/cm^3. Influence of sintering temperature on YS is relatively small at all density levels.

The reference material C-08C shows UTS values between 550 MPa (7.1 g/cm^3) and 770 MPa (7.5 g/cm^3) after sintering at 1120°C. The gain in UTS with higher sintering temperature is comparable to that of the other materials, i.e. 5-15% higher UTS after sintering at 1200°C compared to 1120°C and 1-5% higher UTS at 1250°C compared to 1200°C. YS of material C-08C is similar (450-475 MPa) for all sintering temperatures at density 7.1 g/cm^3. At density 7.3 g/cm^3, there is no significant difference in YS (520-530 MPa) after the sintering at 1120°C and 1200°C, while YS has increased to 550 MPa after sintering at 1250°C. The YS of C-08C is 560-595 MPa at the highest density level (7.5 g/cm^3) and the highest value is reached after sintering at 1200°C.

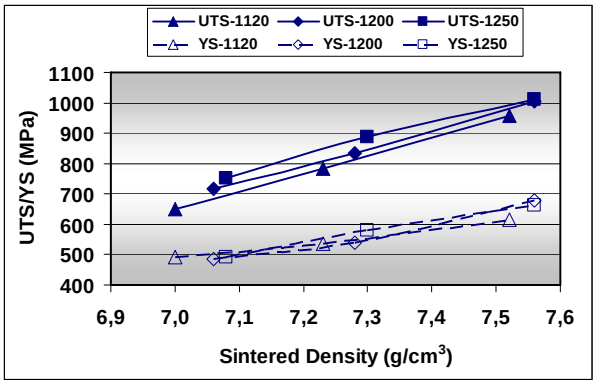

a) UTS and YS for material A-08C

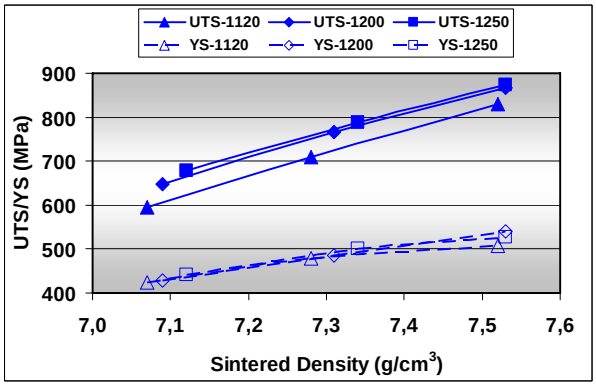

b) UTS and YS for material B-08C

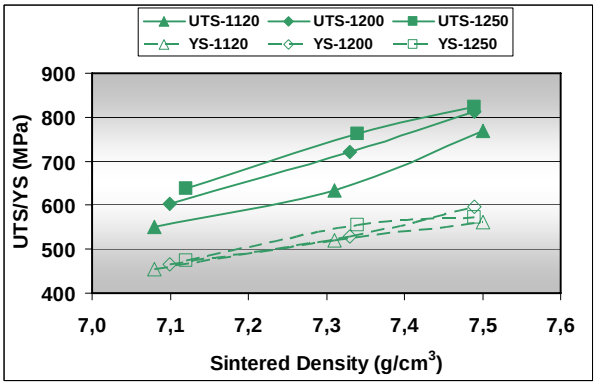

c) UTS and YS for material C-08C

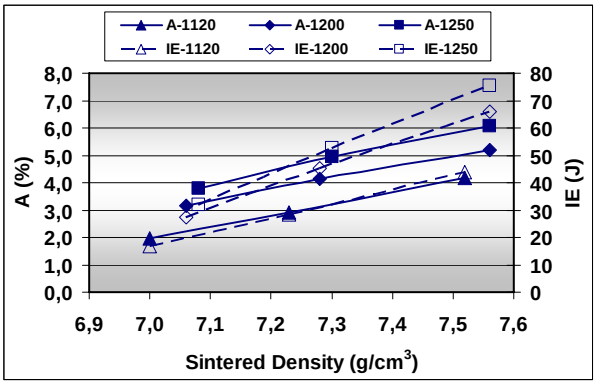

d) A and IE for material A-08C

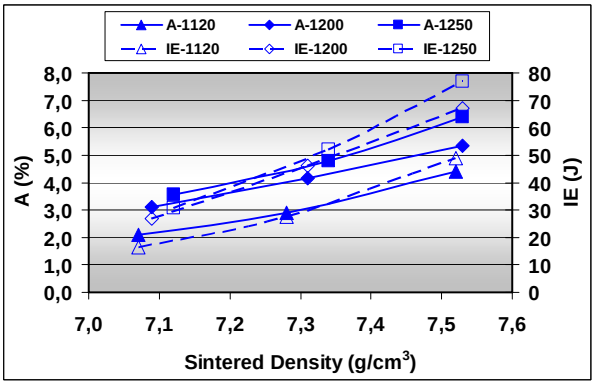

e) A and IE for material B-08C

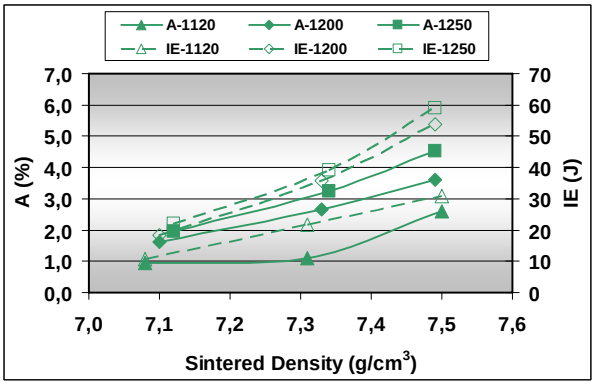

f) A and IE for material C-08C

Fig.4. Mechanical properties obtained after sintering for 30 min at 1120/1200/1250°C in $90N_2/10H_2$ atmosphere (UTS = ultimate tensile strength, YS = yield strength, A = elongation, IE = impact energy).

Materials A-08C and B-08C have very similar elongation fracture (A) and impact energy (IE) properties, as illustrated by graphs d and e in Fig.4. The A values increase from around 2% at the density range 7.0-7.1 g/cm^3 to about 3% at 7.2-7.3 g/cm^3 and further to just above 4% at the highest density (7.5 g/cm^3) after sintering at 1120°C. These elongation

values are considerably enhanced when the higher sintering temperatures are applied. Sintering at 1200°C results in A values that increase from 3.1-3.2% at density 7.1 g/cm^3 to 5.2-5.3% at the density range 7.5-7.6 g/cm^3. Correspondingly, the elongation goes from 3.6-3.8% at density 7.1 g/cm^3 to 6.1-6.4% at the density range 7.5-7.6 g/cm^3 after sintering at 1250°C. The impact strength of materials A-08C and B-08C is significantly improved with higher density for all three sintering temperatures. After sintering at 1120°C, the IE values increase from 16-17 J at densities of 7.0-7.1 g/cm^3 to 44-49 J at density 7.5 g/cm^3. Sintering at 1200°C gives much higher IE values than sintering at 1120°C, while there are smaller differences in IE values between the two high temperature sintering. After these sintering at 1200/1250°C, both materials have IE in the range 27-32 J at density 7.1 g/cm^3 and 66-77 J at the highest density level (7.5-7.6 g/cm^3).

Material C-08C has lower elongation and impact energy values than the other two materials (see graph f in Fig.4). After sintering at 1120°C, elongation is around 1% at both density 7.1 and 7.3 g/cm^3 but increases to 2.6% at density 7.5 g/cm^3, while IE increases linearly with density from 11 J at 7.1 g/cm^3 to 31 J at 7.5 g/cm^3. Both A and IE values are considerably enhanced after sintering at 1200°C compared to the 1120°C sintering. There is also some improvement in these properties after sintering at 1250°C compared to those after 1200°C. The sintering at 1200/1250°C give A values that increase from 1.6-2.0% at density 7.1 g/cm^3 to 3.6-4.5% at density 7.5 g/cm^3, and IE values that goes from the 18-22 J at 7.1 g/cm^3 up to the 54-59 J at 7.5 g/cm^3.

The scatter in the results from the evaluation of mechanical properties was relatively low for all materials. The standard deviation values were in the ranges of 3-12 HV10 (hardness), 0.3-7.0 J (IE), 3-17 MPa (UTS), 4-39 MPa (YS), and 0.1-0.5% (A).

Microstructures

The sintered specimens of materials A-08C and B-08C have microstructures that consist of fine pearlite mixed with some areas of coarser pearlite (see Fig.5). The structures of material B-08C also contain small amounts of ferrite. In the specimens of material C-08C the microstructure is fully upper bainitic. There are no significant differences in microstructure composition between specimens with different densities or between specimens sintered at different temperatures for any of the three materials. The specimens show no obvious signs of surface decarburization.

Some small oxide inclusions are observed in the as-polished microstructures of all specimens of materials A-08C and B-08C after sintering at 1120°C. These oxide inclusions are typically of sub-micrometer size and are mainly found along boundaries between former powder particles, as can be seen in Fig.6a. Specimens with densities in the range of 7.0-7.3 g/cm^3 have about the same amount of oxide inclusions; while the high density (7.5 g/cm^3) specimens have slightly more oxide inclusions (see Fig.6b). There are oxide inclusions visible in the structures of the high density specimens also after sintering at 1200°C as well as after 1250°C (see Fig.6d), although fewer than in the 1120°C sintered samples. In all high density specimens, some larger (up to a few micrometer in size) oxide particles appear occasionally trapped inside pores. The specimens of materials A-08C and B-08C with densities in the range 7.0-7.3 g/cm^3 have only traces of oxides in the structures after sintering at 1200°C and no visible oxide inclusions after sintering at 1250°C; see Fig.6c. None of the sintered specimens of material C-08C have any visible oxide inclusions in the as-polished microstructures.

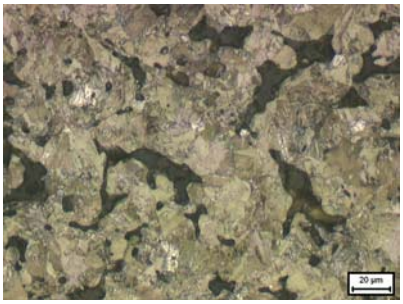

a) material A-08C

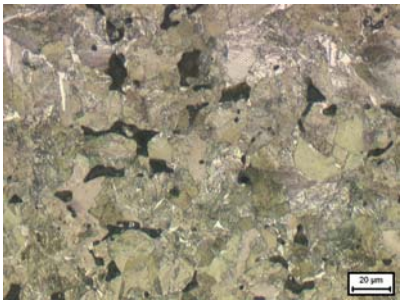

b) material B-08C

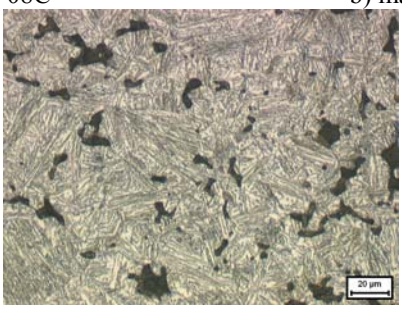

c) material C-08C

Fig.5. Etched microstructures of test specimens with density 7.0-7.1 g/cm^3. The specimens were sintered for 30 min at 1120°C in $90N_2/10H_2$ atmosphere.

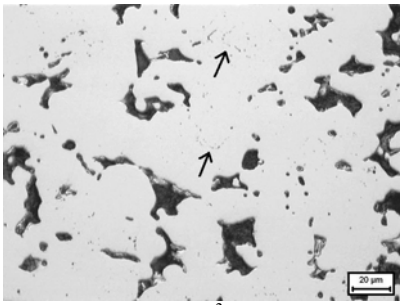

a) ρ = 7.00 g/cm^3, T = 1120°C

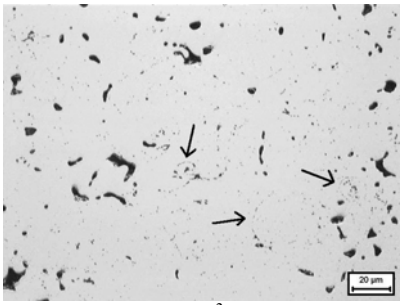

b) ρ = 7.52 g/cm^3, T = 1120°C

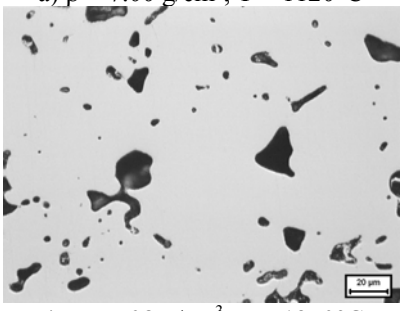

c) ρ = 7.08 g/cm^3, T = 1250°C

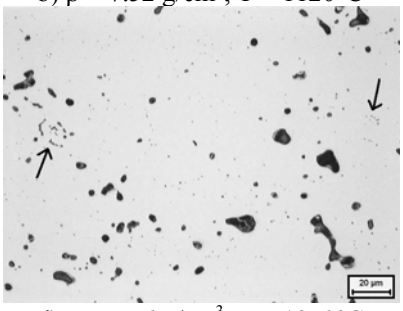

d) ρ = 7.56 g/cm^3, T = 1250°C

Fig.6. As-polished microstructures of material A-08C specimens with density ρ. The specimens were sintered for 30 min at T in $90N_2/10H_2$ atmosphere. Oxides in the structures are marked by arrows.

The pore characteristics are similar in all three materials. The general effects of sintering temperature and sintered density can be seen from the micrographs of material A-08C. Specimens sintered at 1120°C have relatively irregular pore shape while specimens sintered at the higher temperatures have more rounded pores. The pore size decreases with increasing specimen density.

Fracture surfaces

Test specimens of materials A-08C and B-08C with density in the range 7.0-7.1 g/cm^3 display mainly ductile inter-particle fracture mode after sintering at 1120°C, as demonstrated in Figs.7a and 7b. Corresponding specimens that were sintered at higher temperatures (1200/1250°C) have fracture surfaces with similar appearance, although some cleavage fracture sites also appear. The specimens with higher densities (7.3-7.6 g/cm^3) of these materials present mixtures of ductile and cleavage fracture, of inter-particle and trans-particle type, for all sintering temperatures (see Figs.7c and 7d). Fracture surfaces of material C-08C specimens have generally more cleavage sites and less ductile fracture sites than the specimens of the other materials.

Examination of the specimen fracture surfaces of materials A-08C and B-08C in higher resolution reveals that round particulate features are present occasionally in the fractured sinter necks of material sintered at 1120°C. These particles are up to about 1 μm in size and lay inside small dimples, as shown in Fig.7e. There are slightly more such particles in the high density (7.5-7.6 g/cm^3) specimens than in the specimens with densities in the range 7.0-7.3 g/cm^3. The pore surfaces of the high density specimens also contain some particulate features (with size up to a few micrometers), while the pore surfaces in the specimens with lower density are clean and basically particle free. The EDX analyses show that the particulate features in material A-08C are Cr-Mn rich oxides. This is demonstrated by the results in Fig.7e. The Cr/Mn content ratio in these oxides is generally close to a factor of 2. It should be noted in this context that the EDX-analysis captures a larger volume than only the oxide particle and it cannot therefore be concluded whether the oxide contains Fe or not. However, the Cr/Mn ratio of about 2 is always consistently found. Some of the particulate features in material B-08C are also Cr-Mn rich oxides of the same type as in material A-08C, while others are mainly rich in Mn and have low Cr content but contain some Si. In the 1250°C sintered specimens (density 7.0-7.3 g/cm^3) the fracture surfaces are practically free from oxide particulate features for both material types. However, very few oxide particles still exist in the sinter necks of the 1200°C sintered specimens of the same density range. These oxides are confirmed by EDX to be of the same type as those in the 1120°C sintered specimens.

The high density (7.5-7.6 g/cm^3) specimens of materials A-08C and B-08C display occasional particulate features in fractured sinter necks and on pore surfaces also after the high temperature sintering. Size and shape of the particles are similar to the oxide features in the 1120°C sintered specimens. The EDX analyses show that these particles are mainly Cr-Mn rich oxides in material A-08C and Mn rich oxides in material B-08C. The oxides generally also contain some Si and Al in the 1250°C sintered specimens.

The fracture surfaces of all material C-08C specimens are clean and basically free from oxide particulate features.

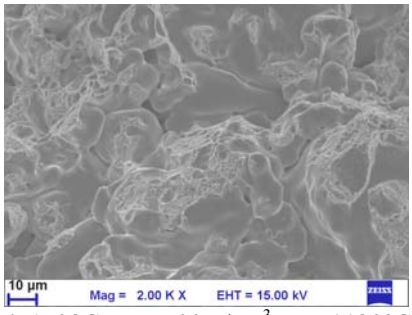

a) A-08C, ρ = 7.00 g/cm^3, T = 1120°C

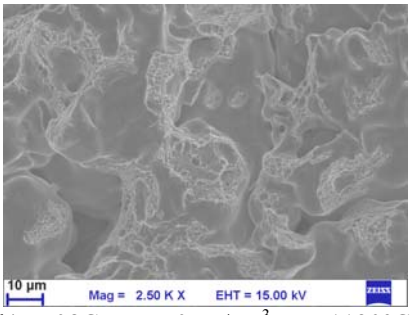

b) B-08C, ρ = 7.07 g/cm^3, T = 1120°C

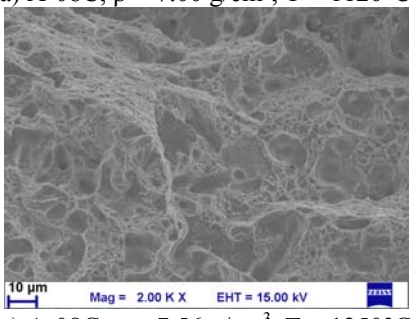

c) A-08C, ρ = 7.56 g/cm^3, T = 1250°C

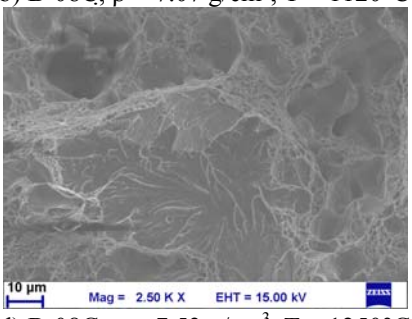

d) B-08C, ρ = 7.53 g/cm^3, T = 1250°C

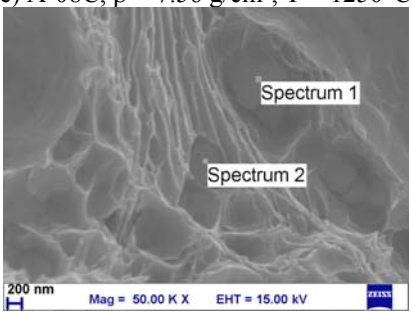

e) A-08C, ρ = 7.52 g/cm^3, T = 1120°C

EDX analysis results in atomic %
(Normalised)

	O	Si	Cr	Mn	Fe
Spectrum1	43.8	1.0	19.8	10.5	24.8
Spectrum 2	42.9	2.3	11.3	5.3	38.2

Fig.7. SEM images of fracture surfaces of TS specimens with density ρ. The specimens were sintered for 30 min at T in $90N_2/10H_2$ atmosphere.

DISCUSSION

The results from the investigation performed show that most of the oxygen in the Cr and Cr-Mn alloy specimens with density 7.0-7.3 g/cm^3 is reduced after conventional sintering at 1120°C in a reducing N_2/H_2 atmosphere. As-sintered bulk oxygen content in these specimens is 0.04-0.05% O, which means that close to 0.1% O has been removed during sintering. Large part of this oxygen should be the oxygen formerly contained in the iron oxide layer on the powder surface, being removed during the heating phase. It has for example been demonstrated that a 7 nm iron oxide layer on typical water atomized powder would mean an oxygen level of about 0.07 wt.% [23]. Clearly, some of the lost oxygen should also be due to reduction of more stable oxides, since clean pore surfaces in the sintered specimens demonstrate that Cr-Mn rich oxide particles that exist on the surfaces of the starting powders have been removed. Such oxide particles are still found entrapped

inside sinter necks of the test specimens and a major part of remaining oxygen should thus be tied up in these oxides after sintering at 1120°C. The EDX analysis results show that entrapped oxides in both materials have Cr/Mn content ratio close to 2, which indicates that they are spinel oxides of type $MnCr_2O_4$ or similar with presence of Fe and small amounts of Si. The Fe content in the oxides cannot be estimated properly as pointed out in the results section, the reason being that the interaction volume in an EDX analysis is larger than the size of the oxide particles.

These findings suggesting the presence of oxide of spinel type are in agreement with thermodynamic calculations on oxide stabilities in the investigated alloys (see Fig.1), where high stability of the spinel oxide phase is predicted. In the B-08C specimens, there are also some entrapped oxides that are Mn-rich and also contain some Si. These might be oxides of another spinel type or of halite type that are being stabilized by the presence of low impurity levels of Si.

As described, the relatively stable Cr-Mn rich oxide particles in the investigated materials are difficult to reduce during sintering at 1120°C. If these oxide particles are present on free surfaces (pore walls) they are, however, readily removed since they then are freely accessible to the atmosphere. Clearly, the interaction with the atmosphere is important for the reduction process since gas species take active part in the reduction reactions, see (1)-(3) in the chapter about oxide reduction during sintering. Still, entrapped oxides in the specimens with density 7.0-7.3 g/cm^3 are reduced at the higher sintering temperatures, resulting in bulk oxygen concentrations of about 0.02% O after sintering at 1200°C and below 0.01% O after sintering at 1250°C. Consequently, there is transport of oxygen from entrapped oxide sites through the steel to nearby pore channels at these temperatures. Reduction of the entrapped oxides should occur through the carbothermal reactions (2) and (3), which is supported by the fact that there is higher carbon loss in the materials during the high temperature sintering than during the 1120°C sintering. Transport of oxygen through the metal by diffusion of the gas species (CO/CO_2) produced in the reduction reactions is unlikely. It is thus expected that diffusion through the metal requires the dissociation of oxygen-containing gases to atomic oxygen. Grabke [24] has shown that the dissociation of CO_2 from reaction (3) into CO gas and adsorbed oxygen is an important mechanism for transfer of oxygen from CO_2-CO mixtures to the metal surface during oxidation or iron, see reaction (5) below. There should now be a driving force for diffusion of the adsorbed oxygen atoms from inside the neck to surrounding pore walls, since the pore surfaces are oxygen-free and in contact with a reducing atmosphere. Oxygen diffuses interstitially through the metal lattice and the atoms are therefore capable of moving fast at high temperatures [25]. The diffusion coefficient D for oxygen in γ-iron has been determined by Takada et al. [26] and it may be expressed as in equation (6), where T is the absolute temperature and R is the molar gas constant. From this expression and equation (7) for calculation of diffusion length x, it is possible to estimate the diffusion time t for oxygen transport through the metal during sintering. The investigated fracture surfaces of sintered specimens show that basically all oxide inclusions inside the necks are within a distance of 10 μm from a pore surface. Diffusion of oxygen atoms this distance takes 0.15 s at the temperature 1200°C and 0.10 s at the temperature 1250°C. These short diffusion times and the fact that there are almost an unlimited number of interstitial diffusion paths through the metal lattice demonstrate that the transport of oxygen atoms from oxide sites to the pore surfaces is very effective during high temperature sintering. Once transported to the pore walls, the oxygen atoms can interact either with carbon atoms on the pore surfaces or with CO and H_2 in the pores and form gas species (CO, CO_2, H_2O) for further transport out of the compacts.

$$CO_2(g) \rightarrow CO(g) + O(ad) \quad (5)$$

$$D = 1.30 \cdot 10^{-4} \cdot \exp\left[-\frac{166(kJ \cdot mol^{-1})}{R \cdot T}\right] m^2 \cdot s^{-1} \quad (6)$$

$$x = 2 \cdot \sqrt{D \cdot t} \quad (7)$$

Equations (6) and (7) show that the time for oxygen diffusion through γ-iron over a distance of 10 μm is short (0.32 s) also at the temperature 1120°C. Consequently, the transport of oxygen atoms from oxide sites to pore surfaces should not be limiting for the reduction process at this temperature either. Furthermore, the availability of carbon in the metal matrix for the carbothermal reduction is not a problem, since carbon has even higher diffusion rate in γ-iron than oxygen. The difficulty to reduce the entrapped oxides during sintering at 1120°C should instead be due to that local thermodynamic conditions at the oxide particles are less favorable for carbothermal reduction of the Cr-Mn spinel oxides than in the case of high temperature sintering. This suggests that a microclimate with suitable CO/CO_2 ratio for reduction is established around the entrapped oxides at the higher sintering temperatures (1200/1250°C), which is not the case at the sintering temperature 1120°C.

The fact that efficient reduction of entrapped stable oxides in the studied materials requires high sintering temperatures in the range 1200-1250°C is well in line with the results from sintering trials performed on PM compacts based on Cr-Mo and Cr-Mn grades of prealloyed powder [13-20]. However, the compacts must have open porosity that enables transport of the oxygen containing gas species out of the compacts; otherwise the reduction processes are stopped [21]. This has been verified by the results obtained for the high density (7.5-7.6 g/cm^3) specimens in this investigation. After sintering at 1120°C, these specimens have bulk oxygen concentrations of 0.08-0.09% O and thereby only around 0.05% O has been removed from the powders in the process. More oxide particles are found entrapped in the sinter necks compared to the specimens with lower density (7.0-7.3 g/cm^3), which is explained by larger contact points between metal particles in the high density specimens. Trapped inside pores in these specimens, there are also some larger Cr-Mn rich oxide features that contribute to the relatively high oxygen content. The bulk oxygen content is somewhat lower (0.05-0.08% O) after the sintering at 1200/1250°C than after the sintering at 1120°C. It is suggested that this difference is a result of the fact that some of the stable oxides are reduced during heating before pore closure occurs. In large, though, the oxide features have similar appearance and occurrence in the high density specimens for all sintering temperatures, but there seem to be some enrichment of impurity elements (Si, Al) in the oxides during sintering at the higher temperatures. It should be pointed out that the sinter necks are well-developed in the high density specimens, which shows that Fe oxide layers on the powder surfaces are effectively reduced during heating and that remaining oxide particulates do not affect the bonding between powder particles established during sintering.

The residual oxides in the sintered specimens of materials A-08C and B-08C have no obvious effect on the evaluated mechanical properties. Both materials gain considerably in mechanical performance with higher sintering temperature in the specimen density range 7.0-7.3 g/cm^3, and it can be assumed that reduction of entrapped oxide particles inside the sinter necks at the higher temperatures contribute to this gain. However, the reference material C-08C attains similar relative gain in mechanical performance with higher sintering temperature as the other materials, although the C-08C specimens are basically

oxide free already after sintering at 1120°C. Moreover, the high density specimens of materials A-08C and B-08C show large improvements in mechanical performance after the high temperature sintering at 1200/1250°C compared to that obtained after the sintering at 1120°C, even though oxide particles remain in the specimens after sintering. Therefore, enhanced mechanical properties with increased sintering temperature for the studied materials mainly results from the increased sintered neck contact area and pore rounding effects. It should be noted here that even if the overall sintered density only changes slightly with increasing sintering temperature, there is a strong local and material redistribution effect at the former powder particle boundaries. The increase in overall sintered density with increasing temperature may have certain effect, but most probably only marginal. About 0.1 g/cm^3 higher density at most (cf. Table 3), cannot provide the observed improvement in tensile strength when comparing the materials sintered at the 1120°C with those sintered at the highest temperature.

As for the influence of specimen density on the mechanical properties, the UTS should increase roughly in linear proportion while elongation and impact strength should increase exponentially with sintered density for PM steel [27]. The results obtained in this investigation correspond relatively well with these correlations. For all three materials, UTS increases nearly linearly with 7-10% for every raise in density with 0.1 g/cm^3 in the range 7.0-7.6 g/cm^3. In the same density range, there is an exponential gain in elongation and impact strength for materials B-08C and C-08C, while these properties increase in a more linear way for material A-08C. The latter could be due to that residual oxides in the high density A-08C specimens have slightly negative effect on the material ductility. However, the mechanical properties are still comparatively very good and similar to those achieved for material B-08C, so the impact of residual oxides at particle boundaries is probably quite small.

When explaining the differences in mechanical performance between the studied materials, their microstructures after sintering need also to be considered. Both the A-08C and B-08C specimens have microstructures that consist of mainly fine pearlite and these structures provide an attractive combination of strength and ductility. The higher hardness and strength of material A-08C compared to material B-08C is explained by somewhat finer pearlitic structure in the former, which is a consequence of the difference in total alloying content between the materials. It is interesting to note that the two materials still have equivalent elongation and impact strength properties, since harder structures usually are less tough. Compared to the reference material C-08C, the mechanical properties of material A-08C are superior in all aspects, while material B-08C has better UTS and ductility, but lower YS values. Hence, the upper bainitic microstructures in the Mo alloyed reference material provide properties that are generally less favorable than those achieved with the fine pearlitic microstructures in the Cr- and Cr-Mn-alloyed materials.

CONCLUSIONS

The conducted study demonstrates that PM steels based on pre-alloyed powder grades with 1.8% Cr and 0.8% Cr-0.4% Mn contain low amounts of oxygen (0.04-0.05% O) after conventional sintering for 30 minutes at 1120°C in reducing N_2/H_2 (90/10) atmosphere. The residual oxygen is mainly in the form of rounded submicron particles consisting of thermodynamically stable Cr-Mn-rich spinel oxides. These oxides originate from particulate features on the powder surfaces that are entrapped between powder particles during sinter neck formation. Application of higher sintering temperatures leads to reduction of the entrapped oxide particles through more active carbothermal reduction mechanisms locally in the materials. Hereby, oxygen concentrations in the materials are

reduced to around 0.02% O after sintering at 1200°C and below 0.01% O after sintering at 1250°C. The conclusions above are valid for test specimen densities in the range 7.0-7.3 g/cm^3 where there is open and communicating porosity in the materials during sintering. Double pressed specimens with very high densities (7.5-7.6 g/cm^3) have relatively high residual oxygen content after 1120°C sintering (0.08-0.09% O) as well as after 1200/1250°C sintering (0.05-0.08% O). This is an effect of pore closure during sintering, which stops oxide reduction at high temperatures by obstructing gas transport processes inside the PM compacts.

The residual oxides have no detrimental effect on the evaluated mechanical properties of the Cr and Cr-Mn PM steels. With carbon content of around 0.7% C after sintering, both alloys have fine pearlitic microstructures that provide attractive combinations of strength and ductility. Somewhat finer pearlite structure in the material alloyed with Cr only gives higher strength (UTS and YS) compared to the Cr-Mn alloy, but the materials still have equivalent elongation to fracture and impact strength. Sintering at 1120°C leads to UTS values of 650/600 MPa and 2% elongation at density 7.0-7.1 g/cm^3. After sintering at 1250°C, these properties are enhanced to UTS values of 750/680 MPa combined with nearly 4% elongation. This gain in mechanical performance with higher sintering temperature is due to pore rounding effects, increased sinter neck contact area, and slightly increased sintered densities. For both materials, UTS obtained after sintering increases roughly linearly with 7-10% for every raise in specimen density with 0.1 g/cm^3 in the range 7.0-7.6 g/cm^3. Gain in elongation with higher density in the same range is also roughly linear for the Cr-alloyed material, while corresponding elongation gain for the Cr-Mn alloy has more exponential character.

Acknowledgements

Assistance from Dr. Eduard Hryha at Chalmers University of Technology in the performance of SEM and EDX analysis is greatly acknowledged. Support from Jenny Westerlund and Heike Grosser at Höganäs AB with experiments and evaluations is also much appreciated.

REFERENCES

[1] Lindberg, C.: Advances in Powder Metallurgy & Particulate Materials, vol. 2, 1999, no. 7, p. 229
[2] Berg, S. In: Proc. of PM2000 World Congress. Vol. 2. Kyoto, Japan, November 2000, JPMA, p. 939
[3] Bergman, O. In: Proc. of Euro PM2003. Vol. 1. Valencia, Spain, October 2003, EPMA, p. 317
[4] Engström, U., Milligan, D., Klekovkin, A.: Advances in Powder Metallurgy & Particulate Materials, vol. 2, 2006, no. 7, p. 21
[5] Bergman, O., Bengtsson, S. In: Proc. of Euro PM2009. Vol. 1. Copenhagen, Denmark, October 2009, EPMA, p. 35.
[6] Karlsson, H., Nyborg, L., Berg, S.: Powder Metallurgy, vol. 48, 2005, p. 51
[7] Chasoglou, D., Hryha, E., Nyborg, L. In: Proc. of Euro PM2009. Vol. 2. Copenhagen, Denmark, October 2009, EPMA, p. 181
[8] Hryha, E., Nyborg, L., Bengtsson, S. In: Proc. of Euro PM2009, Copenhagen. Vol. 2. Denmark, October 2009, EPMA, p. 169
[9] Nyborg, L., Olefjord, I.: Key Engineering Materials, vol. 29-31, 1989, p. 9
[10] Nyborg, L., Norell, M., Olefjord, I.: Surface and Interface Analysis, vol. 19, 1992, p. 607

[11] Kjellqvist, L.: Doctoral Thesis in Materials Science. Stockholm : KTH Royal Institute of Technology, 2009
[12] Bergman, O.: Powder Metallurgy, vol. 50, 2007, n o. 3, p. 243
[13] Ortiz, P., Castro, F.: Materials Science Forum, vol. 426-432, 2003, p. 4337
[14] Castro, F., Ortiz, P. In: Proc. of Euro PM2003. Vol. 1. Valencia, Spain, October 2003, EPMA, p. 261
[15] Ortiz, P., Castro, F.: Powder Metallurgy, vol. 47, 2004, p. 291
[16] Danninger, H., Gierl, C., Kremel, S., Leitner, G., Jaenicke-Roessler, K., Yu, Y.: Powder Metallurgy Progress, vol. 2, 2002, p. 125
[17] Kremel, S., Danninger, H., Yu, Y.: Powder Metallurgy Progress, vol. 2, 2002, p. 211
[18] Hryha, E., Cajkova, L., Dudrova, E., Nyborg, L. In: Proc. of Euro PM2008. Vol. 1. Mannheim, Germany, October 2008, EPMA, p. 109
[19] Bergman, O., Frisk, K., Nyborg, L. In: Proc. of Euro PM2009. Vol. 3. Copenhagen, Denmark, October 2009, EPMA, p. 239
[20] Jaliliziyaeian, M., Gierl, C., Danninger, H.: Advances in Powder Metallurgy & Particulate Materials, 2008, no. 5, p. 72
[21] Danninger, H., Xu, C. In: Proc. of Euro PM2003. Vol. 1. Valencia, Spain, October 2003, EPMA, p. 269
[22] Dlapka, M., Danninger, H., Gierl, C., Lindqvist, B. In: Proc. of Euro PM2009. Vol. 3. Copenhagen, Denmark, October 2009, EPMA, p. 317
[23] Hryha, E., Gierl, C., Nyborg, L., Danninger, H., Dudrová, E.: Applied Surface Science, vol. 256, 2010, p. 3946
[24] Grabke, HJ.: Materials Science Forum, vol. 154, 1994, p. 69
[25] Meijering, JL.: Acta Metallurgica, vol. 3, 1955, p. 157
[26] Takada, J., Yamamoto, S., Kikuchi, S., Adachi, M.: Metallurgical Transactions A, vol. 17, 1986, p. 221
[27] Höganäs Handbook for Sintered Components, Part 3 – Design and mechanical properties. Höganäs AB, 1997